Nanoscale

PAPER

View Article Online
View Journal | View Issue

Cite this: *Nanoscale*, 2023, **15**, 8197

Elaborating the interplay between the detecting unit and emitting unit in infrared quantum dot up-conversion photodetectors

Qiulei Xu, Xinxin Yang, Jiao Jiao Liu, Fei Li, Ruiguang Chang, Lei Wang, A Qiang Wang,* Zhenghui Wu,* Huaibin Shen and Zuliang Du

The quantum dot up-conversion device combines an infrared photodetector (PD) and a visible quantum-dot light-emitting diode (QLED) to directly convert infrared targets to visible images. However, large efficiency loss is usually induced by the integration of the detecting unit and the emitting unit. One of the important reasons is the performances of the PD and QLED units restraining each other. We regulated the equilibrium between infrared absorption and visible emission by changing the thicknesses of infrared active layers in up-conversion devices. A good balance could be achieved between the absorption of 980 nm incident light and the out-coupling of the 634 nm emission when the active layer thickness is 140 nm, leading to the best performance of the up-conversion device. As more photogenerated carriers are produced with the increase of infrared illumination intensity, the external quantum efficiency (EQE) of the QLED unit in the up-conversion device remains little changed. This suggests the limited amount of photogenerated holes in the PD unit does not limit the EQE of the QLED unit. However, a PD unit with a high ratio of photogenerated holes trapped near the interconnection decreased the EQE in the QLED unit. This work provides new insights into the interplay between the PD and QLED units in up-conversion devices, which is crucial for their further improvements.

Received 17th March 2023,
Accepted 12th April 2023

DOI: 10.1039/d3nr01237a

rsc.li/nanoscale

1. Introduction

The infrared up-conversion photodetector integrating the infrared photodetector (PD) and the visible light emitting diode enables the conversion of infrared light into visible light. Thus, it can convert the infrared targets into visible images directly seen by the naked eye or digital equipment without a complex readout circuit, which promises important applications in the fields of night vision, semiconductor wafer detection, gesture recognition, 3D and biological imaging.[1–3] However, the current high-performance infrared up-conversion detectors are mainly based on complex device structures or expensive film deposition techniques,[4–7] which limit their practical applications. Colloidal quantum dots (CQDs) are promising nano-semiconductor materials, which are characterized by size-tunable bandgap and solution processibility.[8–10] Among them, lead sulfide (PbS) CQDs exhibit excellent capabilities of photon–electron conversion, and the absorption wavelength can be extended to the short-wave infrared region (1–2.7 μm). The incident photon-to-electron conversion efficiency (IPCE) of the conventional photodiode (PD) based on PbS CQDs has reached 80%,[11–13] while the external quantum efficiency (EQE) of the visible quantum-dot light emitting diodes (QLEDs) has also exceeded 25%.[14–16] Therefore, the infrared up-conversion device combining the PbS-based PD and visible QLED has great advantages in achieving fast and low-cost infrared imaging.

In 2011, Franky So's group fabricated up-conversion devices by inserting the PbSe CQDs active layer at the anode interface in organic light-emitting diodes (OLEDs).[17] Later, they improved the device performance by replacing the PbSe layer with the PbS layer.[18] However, these devices showed turn-on voltage beyond 6 V, and the photon–photon conversion efficiency (η_{pp}) was less than 1.3% with high working bias (>10 V), where η_{pp} is equal to the product of IPCE and EQE of the up-conversion device. In 2016, they introduced a high-gain vertical PbS-based phototransistor with IPCE of up to 1×10^5%.[5] While it was integrated with an OLED to form an up-conversion device, the η_{pp} was limited to 1000% due to the <1% EQE of the OLED unit. With the development of synthetic techniques of CQDs and the device structure design, QLEDs

Key Laboratory for Special Functional Materials of Ministry of Education, National & Local Joint Engineering Research Centre for High-efficiency Display and Lighting Technology, School of Materials and Engineering, Henan University, Kaifeng 475004, China. E-mail: wuzhenghuihk@henu.edu.cn, wms835955615@henu.edu.cn

demonstrated impressive efficiency and stability, which already showed more desired merits than OLEDs. In 2019, Sun's group first integrated a QLED and a PbS-based photoconductor to fabricate infrared up-conversion devices.[19] As a result, a low turn-on voltage of 2.5 V was realized with a maximum η_{pp} of over 3% at 970 nm. The η_{pp} was further improved to 6.5% by replacing the PbS-based photoconductor with a PbS-based photodiode by Ning's group in 2020.[20] Based on trap-assisted carrier tunnelling from the electrode, the PbS-based photodiode achieved an IPCE of over 900% due to high photocurrent gain. Nevertheless, when the PbS photodiode was integrated into the up-conversion device, the η_{pp} was only 6.5%, since both the PD unit nor the QLED unit did not work as excellently as they work independently.[21] The previous works frequently demonstrated that the emitting unit integrated into the up-conversion device did not perform as excellently as it performed separately. This suggested that the performances of the detecting unit and emitting unit in the infrared up-conversion devices actually constrain each other, causing huge efficiency loss after integration. However, the interplay between the PD unit and QLED unit in the up-conversion devices has not been sufficiently studied.

In this work, we investigated the interplay between the PD unit and QLED unit in the infrared up-conversion devices from the perspectives of optics and carrier dynamics. In our device structures, the incident of the infrared illumination and the emitting of the visible light were from the same side of the up-conversion device. The emitted light from the QLED unit was inevitably partially absorbed when it passed through the PbS layer, which also had strong absorption in the visible spectrum. Thus, we investigated the balance between the photogeneration of carriers in the PbS infrared active layers and the outcoupling of the emission from the QLED unit by tuning the thickness of the PbS layers. As a result, we found that the optimal thickness of the PbS functional layer was 140 nm. Though the infrared absorption in 140 nm PbS was not the highest, it allowed moderate light outcoupling on the other hand. In addition, we also investigated the impacts of the interplay between PD and QLED units on the carrier injection and radiative recombination in the QLED unit in the up-conversion devices. Electrons were externally injected into the QLED unit from the Al electrode, which was usually highly efficient. However, holes were first generated in the PbS layer and then injected into the QLED unit, leading to limited amounts of holes available for the injection. We varied the amounts of photogenerated holes in the same up-conversion device by adjusting the infrared illumination intensity. We found that only varying the amounts of photogenerated holes did not affect the radiative recombination efficiency in the QLED unit. On the other hand, when a high ratio of photogenerated holes was trapped and accumulated in the PD unit, the EQE of the QLED unit was reduced. The conclusions drawn in this work provide valuable insights into the loss mechanisms related to the integration of PD and QLED units in the up-conversion devices.

2. Results and discussion

The device structure of the up-conversion photodetector in this work is schematically shown in Fig. 1(a). The up-conversion device consisted of a PbS CQDs-based detecting unit and a cadmium selenide (CdSe) CQDs-based emitting unit. The ZnO layer deposited on the ITO substrate was used to extract photogenerated electrons from the PbS active layer under infrared illumination and block hole injections from the ITO electrode. The PbS CQDs solution with 1st excitonic absorption peak at 980 nm was chosen to prepare the photosensitive layer, as shown in Fig. 1(b). Photogenerated holes were injected into the QLED unit for radiative recombination with the assistance of photovoltage generated in the PD unit as well as the externally applied voltage. TFB worked as a hole transport layer (HTL) and was an important interface layer to extract the photogenerated holes from the PbS layer and inject them into the CdSe emitting layer. The device fabrication and basic characterization techniques were referred to in previous works.[20,21] The emission peak of the CdSe CQD layer was at 634 nm, as shown in Fig. 1(c). As shown in Fig. 1(b), the PbS layer also had strong absorption at 634 nm. The second ZnO layer next to the Al electrode was used as an electron transporting layer for the QLED unit. Under infrared illumination, the photogenerated holes injected from the TFB side and the externally injected electrons from the ZnO/Al electrode were radiatively recombined in the CdSe emitting layer, so that the up-conversion device was turned on. While in dark, there were no photogenerated holes in the PbS layer, and the external hole injection was also blocked by the bottom ZnO layer. As a result, there was no radiative recombination in the QLED unit and the up-conversion device was in the "off" state. The number of photogenerated holes in the PD unit under infrared

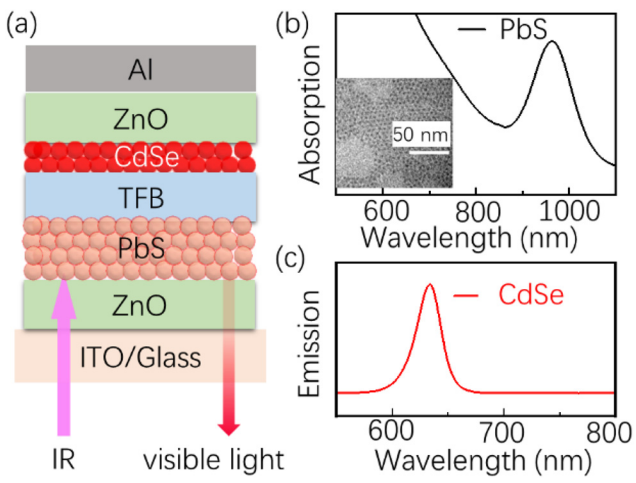

Fig. 1 (a) Device structure of a typical quantum-dot-based infrared up-conversion photodetector; (b) the absorption spectrum of PbS CQDs with a first excitonic absorption peak at 980 nm, the inset is a transmission electron microscopy (TEM) image of PbS CQDs; (c) photoluminescence spectrum of cadmium selenide (CdSe) CQDs with a peak at 634 nm.

illumination is greatly determined by the luminance and the brightness of the visible emission in the up-conversion device.

Usually, a thicker PbS layer can absorb more infrared light and generate more holes for radiative recombination in the QLED unit. However, thicker PbS may also decrease the light outcoupling from the up-conversion device. On the other hand, more injected photogenerated holes may also affect the interplay between the PD unit and the QLED unit from the perspective of carrier dynamics. Therefore, the thickness of the PbS layer in up-conversion devices is a key parameter to regulate the interplay. Firstly, the thickness of the PbS layer was varied from 60 nm to 180 nm to find the balance between the infrared absorption and outcoupling of visible emission. Fig. 2(a) and (b) shows the current density (J)–voltage (V)–luminance (L) characteristics of the up-conversion devices under dark or infrared illumination when the thickness of the PbS layer is increased from 60 nm to 180 nm. As shown, the devices showed very low dark current density without infrared illumination, which was about 10^{-5} mA cm^{-2} at zero bias. The dark current density slightly increased as the driving voltage increased due to small amounts of intrinsic carriers and a slight leakage current. The dark current was less than 0.7 mA cm^{-2} even at a high bias of 8 V, suggesting a good hole-blocking effect of the ZnO layer and an electron-blocking effect of the TFB layer. As the thickness of the PbS layer increased, the dark current slightly increased, which might be due to the morphological cracks generated through the multiple times of solid-state ligand exchanges. The power density of the 980 nm incident infrared light was measured to be 9.5 mW cm^{-2}. Under infrared illumination, the current density climbed up rapidly before 3.5 V and was then gradually saturated. The fast increase in current density was a result of enhanced extraction of the photogenerated holes with the assistance of an external electric field. As the applied bias exceeded 3.5 V, nearly all the photogenerated holes were injected into the QLED unit and the current density thus reached saturation. We observed the same trend in the luminance–voltage characteristics of the up-conversion devices. The saturation current was determined by the IPCE of the PD unit and illumination intensity. The saturation luminance was affected by both the saturation current and the EQE of the QLED unit. With infrared illumination, the saturated photocurrent densities of the up-conversion devices increased as the PbS layer thickness increased from 60 nm to 180 nm, which was attributed to enhanced absorption of the infrared light and thus the increased number of the photogenerated carriers. However, the photocurrent density did not linearly increase with the thickness of the PbS layer, due to the optical interference in the devices.[22] In contrast, we observed that the luminance did not always increase as the thickness of the PbS layer increased. As summarized in Table 1, when the PbS layer thickness was 60 nm, the up-conversion devices exhibited a saturated luminance of 210 cd m^{-2}, which slightly declined to 194 cd m^{-2} as the thickness changed to 100 nm, and then it went up to 306 cd m^{-2} at 140 nm and rapidly dropped to 242 cd m^{-2} at 180 nm finally.

To explain why the luminance of the up-conversion devices sometimes decreased when more holes are photogenerated in a thicker PbS layer and injected into the QLED unit, we calculated the IPCE of the PD unit and the EQE of the QLED unit for the up-conversion device, which are shown in Fig. 2(c) and (d). Some of the key figure-of-merits of the up-conversion devices are summarized in Table 1. It should be noted that the IPCE of the PD unit and the EQE of the QLED unit were both measured from the same up-conversion device, rather than from the separate PD or QLED. As shown in Table 1, the saturated IPCE of the up-conversion devices, which was usually linearly related to the illumination power absorbed by the PbS layer, kept increasing as the thickness of the PbS layer increased from 60 nm to 180 nm. Especially, the absorption percentage increased fast as the thickness of the PbS layer increased from 100 nm to 140 nm. According to previous simulation studies on the absorption of a photosensitive layer sandwiched between multiple thin films, constructive optical interference should be achieved for 980 nm light when the thickness of the PbS layer was about 140 nm.[23,24] As the thickness of the PbS layer increased further, the absorption and IPCE increased slowly and gradually approached the theoretical maximum. On the other side, the EQEs of the QLED units in the up-conversion devices monotonically decreased as the thickness of the PbS layer increased. The EQE was only 11.1% even if there was only a 60 nm PbS layer. As a comparison, the maximum EQE of the typical QLEDs based on the same CdSe

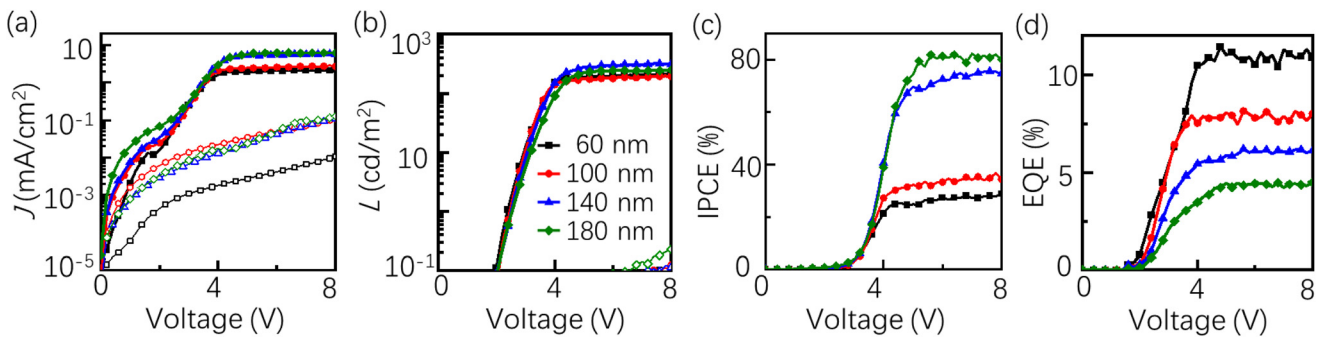

Fig. 2 (a) Current density (J)–voltage (V) characteristics (b) luminance (L)–voltage (V) characteristics (c) IPCEs of the PD units (d) EQEs of the QLED units in the up-conversion devices with different PbS thicknesses.

Table 1 Performance of up-conversion devices with different PbS thicknesses. The photocurrent J_{ph} = J (with infrared illumination) − J (in dark)

Thickness of PbS	Saturated η_{pp} (%)	Saturated L (cd m^{-2})	Saturated J_{ph} (mA cm^{-2})	Saturated EQE (%)	Saturated IPCE (%)
60 nm	3.1	210	2.11	11.1	28
100 nm	2.9	194	2.65	8.0	36
140 nm	4.5	306	5.65	6.0	75
180 nm	3.6	242	6.18	4.4	81

CQDs and similar device structure was about 22%. When the thickness of the PbS layer was about 140 nm, a good balance between the IPCE and EQE was achieved, leading to an optimized η_{pp} of 4.5%. The differences in the EQE of the up-conversion devices with different thicknesses of the PbS layers are supposed to be caused by the re-absorption of the visible emission in the PbS layer, possibly as well as the change of the radiative recombination efficiency in the CdSe layer. Next, we examined these two factors one by one.

As seen from the transmittance spectra of the PbS film coated on glass with different thicknesses in Fig. 3(a), the visible light transmittance of the PbS film at 634 nm dropped from 66% to 32% as the thickness increased from 60 nm to 180 nm. However, the actual transmission percentages of the visible emitted light from the up-conversion devices should be significantly different from those measured from the single layer of PbS coated on the glass substrate, considering the optical interferences in the multiple layers of thin films in the up-conversion device. We designed devices with the new structure for optical measurements, as shown in Fig. 3(b), so that the visible emitted light from this new structure and from a QLED unit of a typical up-conversion device experienced a similar optical path. The thickness of each layer in the device ITO/ZnO/PbS/TFB/CdSe was exactly the same as that in the up-conversion device. Monochromatic light with a wavelength of 400 nm was shed on the device from the CdSe side. The CdSe CQDs emitted 634 nm light upon excitation by the 400 nm incident light. Before the visible emission was detected by the silicon photodiodes, it passed through multiple thin films similar to those in up-conversion devices. A long pass filter with a cut-on wavelength at 520 nm was placed between the sample and the silicon photodiode to block the 400 nm incident light. As the thickness of the PbS layer varied from 0 to 220 nm, the photocurrent generated by the silicon photodiode continuously decreased from about 9.5 nA to 1.3 nA as shown in Fig. 3(c), which confirmed the great impacts of the re-absorption of visible emission on the performance of up-conversion devices. When the sample without the CdSe emitting layer was measured, the photocurrent of the silicon photodiode was <10 pA, which indicated that the incident 400 nm light was almost completely blocked by a long pass filter. From the comparison between the impacts of the thickness of PbS on the EQE of the up-conversion device and the transmission of the visible emission through the multiple thin films, as shown in Fig. 3(c), the decreasing trends observed in EQE as well as in the transmission of emitted light were almost the same. This suggested that the re-absorption alone could almost fully explain the drop of EQE in the up-conversion devices with a thicker PbS layer. It is possible to design optical structures, such as microcavity, to reduce the re-absorption of visible light. On the other hand, it is also promising to design a new device that is illuminated with NIR light from one side and gives out visible light from the other side. Whether the amounts of photogenerated holes affected the radiative recombination and EQE of the QLED unit would be examined more directly next.

The number of photogenerated holes was varied by changing the infrared illumination intensity. The intensity-dependent characteristics were measured from the same up-conversion device so that any other factors possibly affecting the EQE

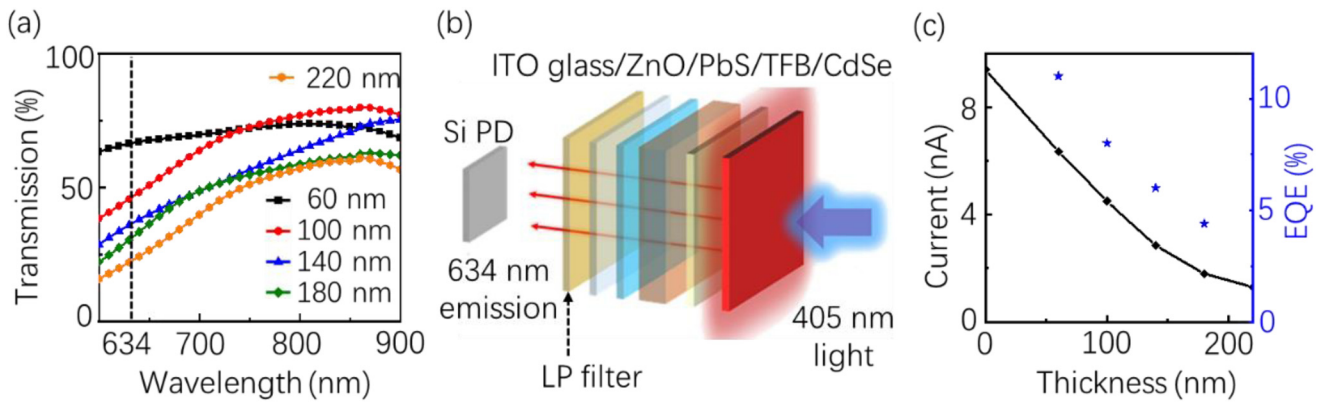

Fig. 3 (a) The transmission spectra of PbS thin films on glass substrates with different thicknesses; (b) schematic configuration of the measurements on the relative outcoupling efficiencies of the up-conversion devices; (c) comparison between the intensities of outcoupled light and EQE of the QLED unit in up-conversion device.

of the QLED unit could be excluded. Fig. 4(a) and (b) showed the current density–voltage–luminance characteristics of the up-conversion device with the 140 nm PbS layer when the infrared illumination intensity increased from 0.6 mW cm^{-2} to 28.7 mW cm^{-2}. The variation range of the number of photogenerated holes due to different illumination intensities fully covered the variation range due to different thicknesses of the PbS layer. As shown in Fig. 4(c), the EQE of the QLED unit in the up-conversion device with illumination intensities higher than 1 mW cm^{-2} varied between 5.8% and 6.2% without a clear trend. This suggested that the less sufficient amount of photogenerated holes compared to the externally injected electrons in the up-conversion device was not a contribution to the efficiency loss caused by the integration of the PD unit and QLED unit. Intuitively, the imbalance between the limited amount of photogenerated holes and the unlimited number of external electrons available for injection into the QLED unit might be one of the main contributors to the loss caused by the integration in up-conversion devices. However, the results from the above experiments were quite different from our intuition. To explain the results contrary to our intuition, we start with the unique working mechanisms of recombination in QLED. According to previous studies on QLED, the electrons, and holes actually are sequentially injected into the CdSe quantum dot.[25] One electron is injected into a CdSe dot first, the second electron cannot be injected until a hole is injected into the dot and recombined with the first electron. Therefore, whether the first injected electron is delocalized and escapes from the dot before it meets an injected hole is one of the key factors determining the EQE of the QLED. In an optimized QLED, the injected electrons can be hardly delocalized under low working bias, and then high EQE closing to the theoretical limit (~20%) can be easily achieved, though injection efficiencies of electrons and holes show moderate differences.[26,27] On the other hand, it should be noted that when the infrared illumination intensity was too low, or only 0.6 mW cm^{-2}, the EQE of the up-conversion device under high bias (~6 V) was just about 5%, which was lower than those measured under higher illumination intensities. When the illumination intensity was <1 mW cm^{-2}, the number of photogenerated carriers was too low. Therefore, the amount of the trapped or accumulated photogenerated holes in the PbS layer or the PbS/TFB interface was significantly higher than that of the injected holes.[28,29] The coulombic attraction between the accumulated holes and electrons in the CdSe layer may delocalize the electrons. Thus, the electrons escaped from the CdSe layer non-radiatively recombined with the trapped holes at the PbS/TFB interface. This kind of recombination loss in the up-conversion device is schematically illustrated by the black ellipse shown in Fig. 4(d). The above non-radiative recombination did not reduce the photocurrent, but reduced the amounts of available hole–electrons pairs for radiative recombination in the CdSe layer, leading to reduced EQE of the up-conversion device. The leakage of electrons becomes more serious with higher bias on the up-conversion device, leading to further decreased EQE. Therefore, the trapping and accumulation of holes at the PbS/TFB interface should be one of the main contributions to the efficiency loss upon the integration of the PD unit and QLED unit, while the total amount of the photogenerated holes available for injection does not make significant differences in the up-conversion devices. The trapping and accumulation of holes not only reduce the EQE of the QLED unit through enhanced non-radiative recombination loss but also may reduce the IPCE of the PD unit through the enhanced bi-molecular recombination between photogenerated holes and electrons. The bi-molecular recombination loss in the up-conversion device is schematically illustrated by the blue ellipse shown in Fig. 4(d). The enhanced bi-molecular recombination in the PD unit upon integration should be another important reason for the low efficiency of the up-conversion devices based on a high-performance PD with >900% IPCE. It should be noted that the turn-on voltages (~2 V) of the up-conversion devices were usually larger than that (~1.7 V) in a similar QLED operated separately, which also indicated that there were significant injection barriers for photogenerated holes in the up-conversion devices. This also increased the probability of hole accumulation at the PbS/TFB interface and the associated delocalization of electrons in the CdSe layer.

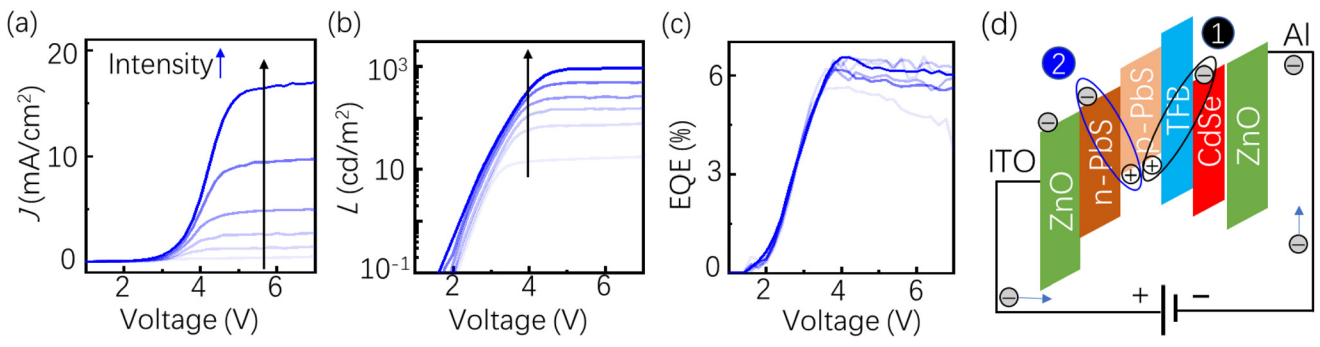

Fig. 4 (a) Current density (*J*)–voltage (*V*) characteristics (b) luminance (*L*)–voltage (*V*) characteristics (c) EQEs of the QLED units in the up-conversion device with 140 nm PbS layer, when the infrared illumination intensities were 0.6 mW cm^{-2}, 2.3 mW cm^{-2}, 4.4 mW cm^{-2}, 8.3 mW cm^{-2}, 8.32 mW cm^{-2}, 16.4 mW cm^{-2}, 28.7 mW cm^{-2}, respectively. (d) Schematic illustration of the two kinds of recombination loss in up-conversion devices.

Our findings imply that suppressing the hole accumulation in the PD unit and reducing the injection barrier at the interface between the PD unit and QLED unit are crucial for optimizing the performance of the up-conversion devices. Reducing the electron injection efficiency in the QLED unit to match the limited amount of photogenerated holes might not achieve significant improvement in the performance of up-conversion devices. This also explains that the up-conversion devices with a reverse device structure (*i.e.*, the photogenerated electrons and external holes are injected into the QLED unit from the PbS/TFB interface and Al electrode, respectively) usually result in no apparent improvement.

3. Conclusions

In summary, this work elaborated on how the infrared detecting unit and the visible emitting unit interact with each other in an up-conversion photodetector. As the thickness of the PbS layer in the PD unit increases to absorb more incident infrared light and generate more photocarriers, the light outcoupling efficiency of the visible QLED decreases significantly. Therefore, optimized performance of the up-conversion device is usually achieved with a thin PbS absorbing layer, or 140 nm in our case, which can balance the photogeneration of carriers and outcoupling of the emitted visible light. On the other hand, the imbalance between the limited amount of photogenerated holes and the unlimited number of external electrons does not cause significant loss upon the integration of the PD unit and QLED unit in the up-conversion device. However, too low a concentration of photogenerated holes in the PD unit leads to lower EQE of the QLED unit. This may be because more trapped holes than injected holes induce the delocalization of electrons in the CdSe layer through coulombic attraction. This implies that the carrier trapping in the PD unit, as well as the possible hole accumulation due to too high injection barrier at the interface between PD and QLED, should be reduced for further improvement of the EQE and the η_{pp} of the up-conversion device. The new insight into the interplay between the PD unit and QLED unit elaborated in this work provides valuable guidance to further optimize the infrared up-conversion photodetector.

4. Experiment section

4.1. Materials

Lead oxide (PbO, >99.9%), hexamethyldisilathiane ((TMS)2S, synthesis grade), octadecene (ODE, 90%, technical grade), oleic acid (OA, 90%, technical grade), *n*-octane (98%), tetrabutylammonium iodide (TBAI, >98%), 1,2-ethanedithiol (EDT, >98.0%) were purchased from Sigma Aldrich. TFB was purchased from Heraeus Deutschland GmbH and Co. KG and American Dye Source, respectively. Ethanol, acetone, and acetonitrile (analytical grade) were purchased from Sinopharm Chemical Reagent Co., Ltd. All the chemicals were used without further purification.

4.1.1. Synthesis of PbS QDs. 2 mmol PbO, 6 mL OA, and 14 mL ODE were loaded in a three-necked bottle and heated to 100 °C for 20 min 0.2 mL $(TMS)_2S$ diluted in 1.8 mL of ODE was quickly injected into the above mixture and kept for 30 s. The reaction solution was cooled to room temperature with ice water. Then, the PbS CQDs were purified using methanol and acetone and finally dissolved in octane (50 mg mL^{-1}) for device fabrication.

4.1.2. Preparation of sol–gel ZnO. 0.5 g $Zn(OAc)_2$ and 0.135 mL ethanolamine were mixed in 10 mL 2-methox-yethanol and stirred vigorously for 12 h in the dark.

4.1.3. Synthesis of ZnMgO nanoparticles. ZnMgO (NPs) were synthesized by solution precipitation method using zinc acetate, magnesium acetate, and tetramethylammonium hydroxide (TMAH). The molar proportion of magnesium acetate was 12.5% of the total metal precursor. For a typical synthesis, a solution of zinc acetate and magnesium acetate in DMSO (0.5 M) and 30 mL of TMAH in ethanol (0.55 M) were mixed and stirred for 1 h in ambient air. Then ZnMgO NPs were washed and dispersed in ethanol at a concentration of 40 mg mL^{-1}.

4.2. Device fabrication

The sol–gel ZnO was spin-cast on top of the pre-cleaned ITO substrates at 2000 rpm and annealed at 200 °C for 20 min, the PbS QDs solution was then deposited layer by layer to obtain the desired film thickness. The first several PbS layers were treated with 10 mg mL^{-1} TBAI in methanol for ligand exchange to prepare the n-PbS film, and the last two layers of the PbS film were treated with 0.02 vol% EDT in acetonitrile solution to prepare the p-PbS film. For each layer, the ligand solution was dropped on and left for 30 s, and then washed with acetonitrile three times to remove the excess ligands. The PbS film was subsequently annealed in air at 80 °C for 10 min before transferring to the glove box. 10 mg mL^{-1} TFB in chlorobenzene was applied on the PbS film and annealed at 80 °C for 10 min followed by spin coating of 18 mg mL^{-1} CdSe QDs at 2500 rpm. The ZnMgO QDs (40 mg mL^{-1} in ethanol) were deposited at 2000 rpm and annealed lat 60 °C for 30 min. Finally, the prepared samples were transferred into a high vacuum chamber for 100 nm-Al cathode deposition. The effective light-emitting area of the devices was 4 mm^2. All devices were encapsulated with UV-curable resin.

4.3. Device measurement

A UV-vis spectrometer (Lambda 950, PerkinElmer), transmission electron microscope (JEOL JEM-2100), and spectrofluorometer (JY HORIBA FluoroLog-3) were used to Obtain the characteristics of the QDs. The *J–V–L* and spectra intensity distribution were achieved using a PhotoResearch PR-735 SpectraScan spectrometer together with a Keithley 2400 as a power supply for analyzing the up-conversion device. A 980 nm laser was used as a NIR illumination source. The power density of the applied NIR light was detected by an 818-ST2-IR

photodetector located at the same position as the emitting area and calculated by the photocurrent read from a Keithley 6485.

Author contributions

Zhenghui Wu conceived and designed the experiments. Qiulei Xu wrote the original manuscript. Fei Li and Jiao Jiao Liu prepared and tested the materials. Xinxin Yang, Qiulei Xu, and Ruiguang Chang fabricated and characterized the devices. A Qiang Wang and Lei Wang instructed the experiments. Zhenghui Wu and Huaibin Shen reviewed and revised the manuscript. Zhenghui Wu and A Qiang Wang supervised the work. Huaibin Shen and Zuliang Du provided financial support and other necessary research resources.

Conflicts of interest

All the authors declare no conflict of interest related to the work presented in the manuscript.

Acknowledgements

All authors contributed to the scientific discussion and modification of the manuscript. This work was financially supported by the National Natural Science Foundation of China (grant numbers: 62204078, 61922028, 62005114, U22A2072, and 61874039). Natural Science Foundation of He'nan Province for Excellent Youth Scholar (No. 232300421092). Open Fund of the State Key Laboratory of Integrated Optoelectronics + (IOSKL2020KF01).

References

1 K. Xu, W. Zhou and Z. Ning, *Small*, 2020, **16**, 2003397.
2 N. Huo, S. Gupta and G. Konstantatos, *Adv. Mater.*, 2017, **29**, 1606576.
3 X. Xiao, K. Xu, M. Yin, Y. Qiu, W. Zhou, L. Zheng, X. Cheng, Y. Yu and Z. Ning, *Appl. Phys. Lett.*, 2020, **116**, 101102.
4 H. Tachibana, N. Aizawa, Y. Hidaka and T. Yasuda, *ACS Photonics*, 2017, **4**, 223–227.
5 H. Yu, D. Kim, J. Lee, S. Baek, J. Lee, R. Singh and F. So, *Nat. Photonics*, 2016, **10**, 129.
6 I. Nikitskiy, S. Goossens, D. Kufer, T. Lasanta, G. Navickaite, F. H. L. Koppens and G. Konstantatos, *Nat. Commun.*, 2016, **7**, 11954.
7 D. Z. Yang, X. K. Zhou, D. G. Ma, A. Vadim, T. Ahamad and S. M. Alshehri, *Mater. Horiz.*, 2018, **5**, 874–882.
8 X. Tang, M. M. Ackerman, M. Chen and P. Guyot-Sionnest, *Nat. Photonics*, 2019, **13**, 277–282.
9 J. Kim, J. Roh, M. Park and C. Lee, *Adv. Mater.*, 2023, e2212220.
10 F. P. G. de Arquer, D. V. Talapin, V. I. Klimov, Y. Arakawa, M. Bayer and E. H. Sargent, *Science*, 2021, **373**, 640.
11 M. Vafaie, J. Z. Fan, A. M. Najarian, O. Ouellette, L. K. Sagar, K. Bertens, B. Sun, F. Arquer and E. H. Sargent, *Matter*, 2021, **4**, 1–12.
12 C. Dong, S. Liu, N. Barange, J. Lee and T. Pardue, *ACS Appl. Mater. Interfaces*, 2019, **11**, 44451–44457.
13 O. Ozdemir, I. Ramiro, S. Gupta and G. Konstantatos, *ACS Photonics*, 2019, **6**, 2381–2386.
14 X. L. Dai, Y. Z. Deng, X. G. Peng and Y. Z. Jin, *Adv. Mater.*, 2017, **29**, 1607022.
15 Y. Z. Deng, F. Peng, Y. Lu, X. T. Zhu, W. X. Jin, J. Qiu, J. W. Dong, Y. L. Hao, D. W. Di, Y. Gao, T. L. Sun, M. Zhang, F. Liu, L. J. Wang, L. Ying, F. Huang and Y. Z. Jin, *Nat. Photonics*, 2022, **16**, 505.
16 J. J. Song, O. Wang, H. B. Shen, Q. L. Lin, Z. H. Li, L. Wang, X. T. Zhang and L. S. Li, *Adv. Funct. Mater.*, 2019, **29**, 1808377.
17 D. Y. Kim, K. R. Choudhury, J. W. Lee, D. W. Song, G. Sarasqueta and F. So, *Nano Lett.*, 2011, **11**, 2109–2113.
18 D. Y. Kim, T. H. Lai, J. W. Lee, J. R. Manders and F. So, *Sci. Rep.*, 2014, **4**, 5946.
19 N. Zhang, H. Tang, K. Shi, W. Wang, W. Deng, B. Xu, K. Wang and X. W. Sun, *Appl. Phys. Lett.*, 2019, **115**, 221103.
20 H. Tang, K. Shi, N. Zhang, Z. Wen, X. Xiao, B. Xu, H. Butt, Z. Pikramenou, K. Wang and X. W. Sun, *IEEE Access*, 2020, **8**, 71041–71049.
21 W. Zhou, Y. Shang, F. P. G. de Arquer, K. Xu, R. Wang, S. Luo, X. Xiao, X. Zhou, R. Huang, E. H. Sargent and Z. Ning, *Nat. Electron.*, 2020, **3**, 251.
22 Z. Wu, B. Wu, H. L. Tam and F. Zhu, *Org. Electron.*, 2016, **31**, 266–272.
23 B. V. Andersson, D. M. Huang, A. J. Moulé and O. Inganä, *Appl. Phys. Lett.*, 2009, **94**, 043302.
24 J. Gilot, I. Barbu, M. M. Wienk and R. A. Janssen, *Appl. Phys. Lett.*, 2007, **91**, 113520.
25 Y. Deng, X. Lin, W. Fang, D. Di, L. Wang, R. H. Friend, X. Peng and Y. Jin, *Nat. Commun.*, 2020, **11**, 2309.
26 H. Shen, Q. Gao, Y. Zhang, Y. Lin, Q. Lin, Z. Li, L. Chen, Z. Zeng, X. Li, Y. Jia, S. Wang, Z. Du, L. S. Li and Z. Zhang, *Nat. Photonics*, 2019, **13**, 192–197.
27 H. Li, Y. Bian, W. Zhang, Z. Wu, T. K. Ahn, H. Shen and Z. Du, *Adv. Funct. Mater.*, 2022, **32**, 2204529.
28 B. Chen, X. Qiao, C.-M. Liu, C. Zhao, H.-C. Chen, K.-H. Wei and B. Hu, *Appl. Phys. Lett.*, 2013, **102**, 193302.
29 L. J. A. Koster, V. D. Mihailetchi, R. Ramaker and A. P. W. M. Blom, *Appl. Phys. Lett.*, 2005, **86**, 123509.